Journal Name

ARTICLE

Iron Nanoparticles-Based Supramolecular Hydrogels to Originate Anisotropic Hybrid Materials with Enhanced Mechanical Strength.

Received 00th January 20xx,
Accepted 00th January 20xx

DOI: 10.1039/x0xx00000x

www.rsc.org/

Rafael Contreras-Montoya,[a] Ana B. Bonhome-Espinosa,[b] Angel Orte,[c] Delia Miguel,[c] Jose M. Delgado-López,[d,e] Juan D. G. Duran,[b] Juan M. Cuerva,[a] Modesto T. Lopez-Lopez,*[b] and Luis Álvarez de Cienfuegos*[a]

Here we report the synthesis and structural characterization of novel iron nanoparticles (FeNPs)-based short-peptide supramolecular hydrogels. These hybrid hydrogels composed of Fmoc-diphenylalanine (Fmoc-FF) peptide and FeNPs were prepared through the self-assembly of Fmoc-FF in a suspension containing FeNPs in the presence or absence of an external magnetic field. Optical images of these hydrogels revealed the formation of FeNPs column-like aggregates when the gels were formed in the presence of a magnetic field. Moreover, the intrincated structure derived from the interwoven of the fiber peptides with these FeNPs column-like aggregates resulted in anisotropic materials, more rigid under shears applied perpendicularly to the direction of the aggregates, presenting under these conditions values of G´ (storage modulus) about 7 times compared to native hydrogel. To the best of our knowledge this is the first example in which the mechanical properties of peptide hydrogels were strongly enhanced due to the presence of FeNPs. A theoretical model trying to explain this fenomenon is presented. Quite interesting CD, FTIR and synchrotron X-ray difraction analysis indicated that the anti-parallel β-sheet arrangement of Fmoc-FF peptide was highly conserved in the hydrogels containing FeNPs. Moreover, FLCS measurements showed that the diffusion of a small solute through the hydrogel network was improved in hydrogels containing FeNPs probably caused by the formation of preferential channels for diffusion. Taken together, our results provide a new method for the synthesis of novel hybrid Fmoc-FF-FeNPs anisotropic hydrogels with enhanced mechanical strength and water-like diffusion behavior, thus easing their application in drug delivery and tissue engineering.

Introduction

Hydrogels are an important class of materials that have found useful technological and biotechnological applications thank to their high water content and diverse mechanical properties. Moreover, these types of materials can be chemically designed to respond to different external stimuli with the intention of provoking in the hydrogel a physical or chemical change, (i.e., altering their mechanical properties or triggering the release of substances, etc.), making them what have been termed “smart materials”.[1] An important category of these stimuli-sensitive hydrogels are magnetic hydrogels or ferrogels (i.e., the combination of hydrogels with micro- and/or nano-magnetic particles (MP) (e.g., γ–Fe_2O_3 , Fe_3O_4 , $CoFe_2O_4$)) that are able to respond to an external magnetic field modifying their properties (from the microstructure, shape and size to the mechanical behavior).[2] The possibility of altering their properties remotely makes them very appealing for multiple applications, such as, pulsatile delivery vehicles, magnetic resonance imaging contrast agents, hyperthermal therapy agents, etc. The properties of these composite materials rely on several factors, such as, the nature of the hydrogel, the type of interaction (physical or chemical) between the fibers and MP, and the concentration, size and distribution of the MP within the hydrogels. Additionally, the method of preparation can also have an influence in the final properties of the ferrogel.[3] Nevertheless, the interesting properties of these materials have been mainly restricted to polymers thank to their great versatility and capacity to modify their structure.

Recently, supramolecular hydrogels composed of small molecules (low molecular weight gelators, LMWG) able to self-assemble by an external stimulus have turned into excellent candidates for the construction of smart and functional materials.[4] The dynamic nature of the non-covalent self-association makes them more prone to be modified by external stimuli, that in most cases promote a change in the macroscopic properties of these materials causing them to evolve into systems that are adaptive to the environment.[5] Short-peptide supramolecular hydrogels are an example of this

[a] Dpto de Química Orgánica, Facultad de Ciencias, Universidad de Granada (UGR), 18071-Granada, Spain. E-mail: lac@ugr.es
[b] Dpto de Física Aplicada, Facultad de Ciencias, (UGR). E-mail: modesto@ugr.es
[c] Dpto de FisicoQuímica, Facultad de Farmacia, (UGR), 18072-Granada, Spain.
[d] Instituto Andaluz de Ciencias de la Tierra (IACT, CSIC-UGR).
[e] Present address: Dpto de Química Inorgánica, Facultad de Ciencias, (UGR).
† Footnotes relating to the title and/or authors should appear here.
Electronic Supplementary Information (ESI) available: Supplementary figures. See DOI: 10.1039/x0xx00000x

kind of materials.[6] These peptides have a strong tendency to self-associate requiring in most of the cases less than 1 wt% to immobilize the aqueous medium. Due to their chemical structure, these compounds are able to form gels by different stimuli or conditions, mainly solvent, pH and/or temperature changes or enzymatic reaction.[6a,7] The stimulus triggers the self-association process and, as a consequence, different stimuli can differently affect the structural and mechanical properties of the resulting gel. In this sense, much effort has been focused in modifying the mechanical properties of these hydrogels since many useful applications depend on the rheological performance of these materials.[8] For example, it is known that dipeptide LMWG derivative gels can be formed by pH and solvent switch and using one or the other stimulus has an effect in the mechanical properties of the gels, even the homogenization techniques and the final solvent content have also an impact.[9] Alternatively, one strategy to modulate the mechanical properties of these hydrogels has been the development of composite materials by the combination of these peptides with others or with different additives. In this sense, the mechanical properties of hybrid hydrogels composed of Fmoc-FF and Fmoc-K, Fmoc-D or Fmoc-S have shown lower elastic moduli[10a] or higher mechanical strength (Fmoc-RGD)[10b] compared to Fmoc-FF alone. The presence of polymers such as, dextrans,[11] agarose,[12] and konjac glucomannan,[13] have shown mixed results, having, in some cases, a decrease in the mechanical properties of the gel (dextrans); an increase in the fracture stress (agarose); and an increase in the stability and mechanical strength (konjac glucomannan). Furthermore, the incorporation of solid nanoparticles, such as: AgNPs,[14] carbon nanotubes (CNTs),[15] and graphene,[16] have also decreased (AgNPs) or increased (CNTs and graphene) the mechanical strength of the hydrogels. Interestingly, the incorporation of solid nanoparticles in the gel matrix can also provide new properties to these materials, such as, antibacterial and/or fluorescence (AgNPs), and electrical conductivity (CNTs). Additionally, certain nanoparticles are able to exert a structural control over the distribution of the supramolecular nanofibers.[17]

Based on these precedents, herein, we report the synthesis and characterization of novel magnetic supramolecular hydrogels composed by the self-association of Fmoc-FF in the presence of different ratios of core-shell Fe nanoparticles with a polyetilenglycol covering (Fe nanoparticles@PEG) under the influence or absence of an external magnetic field. Our results indicate that when they were prepared under an applied magnetic field, these magnetic hydrogels improve dramatically, up to 7 times, their mechanical properties (measured under shear applied perpendicular to the field direction) with respect to the nonmagnetic, or randomly oriented magnetic nanoparticles hydrogels, whilst, at the same time, the diffusion of a solute through the structure is improved. This improvement in their mechanical properties happens only when the gel is formed in the presence of an applied magnetic field and is the consequence of a particular combination of structural characteristics in the hydrogel. These structural characteristics imply the engulfment of magnetically oriented FeNPs column-like structures by the peptide fibers that have been formed in the presence of them (see Figure 1). We have checked that this anisotropy at the microscopic level is also reflected in the macroscopic mechanical properties of the magnetic hydrogels, which present weaker rheological moduli when the applied shear is within the same plane of the FeNPs column-like structures.

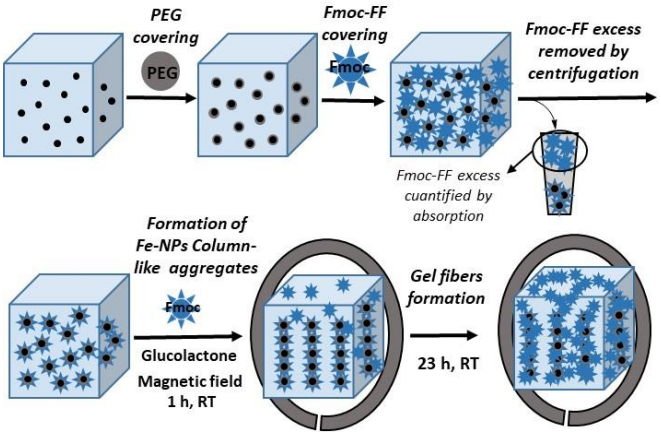

Figure 1. Sketch of the preparation protocol of magnetic hydrogels.

Quite interesting, the non-covalent nature of this self-association allows the inclusion of these FeNPs column-like structures within the peptide network to give a homogeneous hybrid material without practically modifying the secondary structure of the peptide. Surprisingly, this 700 % improvement of the mechanical properties of magnetic hydrogels takes place for a tiny (0.6 vol.%) amount of FeNPs. The simple embedment of the FeNPs within the matrix of the hydrogel cannot justify such a large enhancement; in fact the classical theory of mechanics of composite materials[18] only predicts an enhancement of the mechanical properties of the order of 1 % when such an amount of spherical particles is embedded within a continuous matrix. We demonstrate in our work that application of a magnetic field to the pre-gel mixture induces the aggregation of FeNPs into column-like structures. The particles within the structures are subsequently engulfed by the gel-forming peptides, in such a way that these structures are maintained even after magnetic field removal, serving as scaffolding for the support and mechanical enhancement of the resulting hydrogels, something that to the best of our knowledge has not been previously reported for biological gels. Moreover, these magnetic hydrogels, similar to Fmoc-FF hydrogel can be extruded through a syringe keeping their gel state.[19] All of these new properties, together with the known biocompatibility and biodegradability of these hydrogels, provide these materials with useful potential applications in several biomedical fields, such as, drug delivery agents and tissue engineering. To gain in-depth insights into the morphological and structural properties of these materials, these hydrogels have been studied by magnetization, optical microscopy, environmental scanning electron microscopy, infrared spectroscopy, circular dichroism, X-ray diffraction and

synchrotron X-ray total scattering, fluorescence lifetime correlation spectroscopy and rheology. It is worth noting, that a magnetic supramolecular hydrogel in which the gel to sol transition is triggered by an external magnetic field has been successfully prepared although a study of its mechanical properties has not been reported.[20]

Experimental

Reagents and materials

N-Fluorenylmethoxycarbonyl diphenylalanine (Fmoc-FF), was purchased from Bachem Co., Switzerland and was used without further purification. Fe nanopowder / nanoparticles, 99.7+%, 60 - 80 nm, were purchased from SkySpring Nanomaterials, Inc., Houston, USA. PEG-400 (polyethylene glycol, 400 $g \cdot mol^{-1}$), glutaraldehyde (25% solution in water), mineral oil and sorbitan sesquioleate were provided by Sigma-Aldrich, USA. n-hexane, min 99% was purchased from Scharlab S.L., Spain. D(+)-Glucono-1,5-lactone 99% was purchased from Alfa Aesar, Germany. Sodium nitrate (for analysis) was purchased from Merck, Germany.

Preparation of magnetic nanoparticles with PEG coating

As magnetic phase, we used iron nanopowders consisting of iron nanoparticles (FeNPs) of a diameter in the range 60-80 nm. In order to avoid corrosion, the manufacturer provides the particles in vacuum bags, that we opened under argon atmosphere to reduce contact with oxygen. Immediately afterwards the nanoparticles were coated with a layer of polyethylene glycol (PEG), which protects from corrosion, as we proved in a previous work.[21] Furthermore, the PEG coating also imparts to the particles the biocompatibility required for biomedical applications. Indeed, coating nanoparticles with a PEG layer reduces the attack by macrophages as has been shown.[22] For the PEG coating we adapted the water-in-oil emulsion method described by Chatterjee et al.[23] Briefly, we prepared a water phase that consisted of a mixture of 200 mg of FeNPs and 1 g of PEG-400 in purified water (Milli-Q quality, Millipore Corporation), previously purged with argon in order to remove oxygen and prevent iron NP from corrosion. This mixture was homogenized by ultrasonic bath for 7 minutes. Separately we prepared the oil phase consisting of 450 mL of hexane, 150 mL of mineral oil and 0.75 mL of sorbitan sesquioleate. Afterwards we mixed both (water and oil) phases and sonicated them for 5 minutes in order to obtain a water-in-oil microemulsion. Subsequently, we added 150 mL of glutaraldehyde under mechanical stirring –note that glutaraldehyde is responsible of the initiation of the polymerization of PEG. The reaction was maintained for 2 hours under mechanical stirring. Finally, the magnetic product was separated by magnetic decantation and repeatedly washed with ethanol and purified water (Milli-Q quality). Pristine iron nanoparticles will be referred to as PMNP (Pristine Magnetic NanoParticles), while PEG-coated iron nanoparticles as MNP@PEG.

Characterization of the nanoparticles

The size and shape of the PMNP and MNP@PEG, were characterized by transmission electron microscopy (TEM). The effectiveness of the PEG coating was confirmed by measuring the electrophoretic mobility at different pHs using a Nano Zs, Zetasizer Instrument (Malvern). For this aim, both PMNP and MNP@PEG nanoparticles were suspended in 1 mM solutions of $NaNO_3$. Then, for each of the powders (pristine and coated), in order to determine their isoelectric point, we adjusted the pH of the suspensions of iron nanoparticles in $NaNO_3$ within precise values within the range 4–11, using 0.1 M solutions of NaOH or HNO_3. Measurements, in triplicate for each sample, were carried out at 25 ^oC using disposable plastic cuvettes.
Finally, we characterized the magnetic properties of the dry nanopowders by using a Quamtum Design NPMS X magnetometer.

NonMagnetic Hydrogel (NMHG) preparation

The NMHG gelification was performed following a previously reported described protocol.[24] Very briefly, Fmoc-FF peptide was weighed into a sample tube and deionised water was added to obtain a final concentration of 0.5% (w/v). This suspension was then sonicated (in a HSt Powersonic 603-ultrasonic bath) for 10 minutes. Little portions of NaOH 0.5 M, were then added by pipette. The solution was vortexed (using a LBX V05 series vortex stirrer) and sonicated after each addition to aid mixing, until a clear solution was obtained at a pH of approximately 10.35 (the pH was measured using HACH sension™ PH3 pH meter. The pH meter was calibrated using pH 4, pH 7 and pH 10 buffer solutions). This solution was diluted with deionised water (or 2.5 nM of the fluorescence dye solution for FLCS studies) to obtain a final Fmoc-FF concentration of 0.3% (w/v). Gelation was then carried out by addition of 2 molar equivalents of glucono-δ-lactone (GdL) to the basic peptide solution and mixing was achieved by vortexing for 5 seconds. According to rheological measurements, full gelification at room temperature was achieved after 12 h.

MNP@PEG@Fmoc-FF nanoparticles preparation

100 mg of MNP@PEG were suspended in 1.5 mL of an aqueous basic solution of Fmoc-FF 0.5% (w/v). The resulting suspension was sonicated during 10 min and then centrifuged during 5 min at 10000 r.p.m. (Sigma 1-14 centrifuge); afterwards the supernatant was removed (see sketch in Figure 1). The quantification of the amount of Fmoc-FF adsorbed on the MNP@PEG was calculated by absorption measurements. For this purpose, absorbance of Fmoc-FF solutions of different concentrations were measured at the maximum of absorption (266 nm), obtaining a good linear relationship between absorbance and concentration. Then, the remaining amount of Fmoc-FF in the supernatant was measured spectrophotometrically using an Analytik Jena SPECORD® 200

Plus and thus concentration was obtained from the interpolation in previous fitting (see Figure S1 of the ESI). From the average of three measurements it was found that the adsorption of Fmoc-FF on the MNP@PEG was of 4.7775 x 10^{-2} g Fmoc-FF per gram of MNP@PEG. To further confirm the Fmoc-FF adsorption on the MNP@PEG we performed measurements of the electrophoretic mobility of the new MNP@PEG@Fmoc-FF particles following a similar protocol to the described for the PEG-coated MNP.

Hydrogels-MNP@PEG@Fmoc-FF composites preparation

To an aqueous basic solution of Fmoc-FF 0.5% (w/v) the proper weighted amount of MNP@PEG@Fmoc-FF particles to obtain the different final concentrations of 0.05 vol.%, 0.1 vol.%, 0.3 vol.%, 0.6 vol.%, and 0.9 vol.%, corresponding to hydrogels MHG-0.05, MHG-0.1, MHG-0.3, MHG-0.6 and MHG-0.9, were added and diluted to a final Fmoc-FF concentration of 0.3% (w/v). This suspension was sonicated during 5 min to give a homogeneous suspension. This suspension was gelified by the addition of GdL, keeping it at room temperature during 24 h. To obtain the hydrogels with FeNPs aligned into column-like structures, after the addition of GdL and during 1 hour the hydrogel was kept under the influence of a vertically applied magnetic field of 15 kA·m^{-1} of strength (we used a solenoid connected to a DC power supply for this purpose), followed by 23 h without the stimulus of the magnetic field at room temperature (Figure 1).

Characterization of the magnetic properties of the hydrogels

We obtained the magnetization curve of the magnetic hydrogels by means of a Quamtum Design NPMS X magnetometer. For this aim, we applied different values of the magnetic field and measured the resulting magnetization of the samples.

Optical microscopy

We analyzed the mesoscopic structure of the hydrogels by direct observation with an optical microscope (Nikon, SMZ800) at 5× magnification. We took photos of hydrogels prepared by different experimental protocols using a CCD camera (Pixelink, Canada) connected to the microscope.

Electron Microscopy

TEM images of FeNPs. The nanoparticles used in this work were studied with a LIBRA 120 PLUS Carl Zeiss. A drop of an ethanolic suspension of PMNP and MNP@PEG was placed on a 300-mesh copper grid. The sample was dried at room temperature for 30 min.

ESEM images of hydrogels. Hydrogels images were performed using a FEI Quanta 400 ESEM equipped with a Peltier effect cooling stage.

Circular dichroism (CD)

The CD spectra were recorded using an Olis DSM172 spectrofotometer with a xenon lamp of 150W. The hydrogels were gelified into a 0.1 mm quartz cell (Hellma 0.1 mm quartz Suprasil®) using the protocol described above. Spectra were obtained from 200 to 320 nm with a 1 nm step and 0.1 s integration time per step at 25 °C. Data shown correspond to the average of 20 measurements.

Fourier transform Infra-red (FTIR) spectroscopy

Spectra were recorded using a Perkin-Elmer Two FTIR ATR spectrometer. The hydrogels and the xerogel were compressed onto the diamond crystal. All spectra were scanned over the range between 4000 and 450 cm^{-1}.

X-Ray Diffraction (XRD)

X-ray diffraction patterns were obtained with a Cu Kα radiation (λ = 1.5418 Å) on a PANalytical X'Pert PRO diffractometer equipped with a PIXcel detector operating at 45 kV and 40 mA. The 2θ range was from 5° to 80° with a step size of (2θ) 0.039°. By varying the scattering angle the explored momentum transfer vector (q) was in the range of 1 < q (nm–1) < 28.0, with q = (4p/k) sin h, where h is the scattering angle. A freshly prepared gel was deposited on a silicon holder and dried overnight prior to data collection.

Synchrotron X-ray Total Scattering

Dried gels were loaded in glass capillaries of 0.8 mm diameter and measured at the X04SA-MS Beamline of the Swiss Light Source (SLS) of the Paul Scherrer Institut (PSI, Villigen, CH). The beam energy was set at 16 keV and the operational wavelength (λ = 0.77627 Å) precisely determined by collecting, under the same experimental conditions, a silicon powder standard [NIST 640c, a0 = 0.54311946(92) nm at 22.5 °C]. A position sensitive single-photon counting MYTHEN II was used as detector. Independent He/air and capillary scattering curves, as well as empty and sample-loaded capillary transmission coefficients, were also measured and used for data subtraction of all extra-sample scattering effects and absorption correction.

Fluorescence Lifetime Correlation Spectroscopy

Fluorescence fluctuation traces of a xanthene derivative dye, 4-methoxy-Pennsylvania Green (**4-OMe-PG**),[25] dissolved at 1 nM concentration in the different hydrogels were collected on a MicroTime 200 instrument (PicoQuant, GmbH), based on an Olympus IX-71 inverted confocal microscope. A 470-nm pulsed laser (PicoQuant LDH-P-C-470), controlled by a "Sepia II" driver, was used as the excitation source, working at a repetition rate of 20 MHz. The emitted fluorescence was collected through the 1.4 NA, 100× oil immersion objective and focused onto a 75-µm pinhole, after passing through a

510dcxr dichroic mirror and a HP500LP cut-off filter (AHF/Chroma). After the pinhole, the fluorescence light was split in two channels by a 50/50 beam splitter, spectrally filtered by a 520/35 bandpass filter (Semrock) for channel 1 or a 550/40 bandpass filter (Thorlabs) for channel 2, and detected in two avalanche photodiode detectors (SPCM-AQR SPAD, Perkin-Elmer). The data acquisition was performed with a TimeHarp 200 time-correlated single photon counting (TCSPC) module, working in time-tagged time-resolved (TTTR) mode.[26] The incorporation of time-resolved fluorescence information within fluorescence correlation spectroscopy measurements has given rise to the so-called fluorescence lifetime correlation spectroscopy (FLCS), in which time-weighted filters are applied during the correlation to discriminate actual fluorescence photons from background noise or scattered light.[27] We performed FLCS cross-correlation (CC) between the two detection channels, as well as FLCS autocorrelation (AC) of the signal on the individual channels. The CC and ACF curves, $g(t)$, were fitted to the anomalous diffusion equation:

$$g(t) = g(0)\left[1+\left(\frac{t}{\tau_D}\right)^{\alpha}\right]^{-1}\left[1+\frac{1}{s^2}\left(\frac{t}{\tau_D}\right)^{\alpha}\right]^{-1/2} \quad (1)$$

where τ_D represents the diffusion time, $g(0)$ is the limiting amplitude, s is the geometrical parameter of the excitation volume (ratio between the vertical and the lateral focal radii), and α is the anomalous diffusion parameter. Subdiffusion effects appear when $\alpha < 1$. Apparent diffusion coefficients, D, were obtained as $s^2/4\tau_D$. In anomalous diffusion, the diffusion coefficients are time-dependent, hence, their values should be only considered apparent and taken as a qualitative approximation.[28] However, they can be useful to analyze the overall behavior and detecting specific interactions between the dye and the gel fibers. The FLCS time filters, cross- and autocorrelations, fittings were performed using the SymPhoTime 32 software (PicoQuant). During the fits, the geometrical parameter s was kept fixed as previously characterized.[29]

The fluorescence fluctuation traces of the dissolved dye were collected by focusing 10 μm inside the hydrogel. At least, 15 traces of 150 seconds were obtained in different points of each hydrogel, containing different mass weight of FeNPs, with the gelification performed in the presence of magnetic field as described above. Appropriate controls of the dye dissolved in the NMHG, and in MHG-0.1 and MHG-0.3 but gelified in the absence of the external magnetic field were also conducted.

Rheological characterization

We characterized the rheological properties of the NMHG and MHGs by using a Haake MARS III controlled-stress rheometer (Thermo Fisher Scientific, Waltham, MA, USA). The experimental characterization of the rheological properties of hydrogels presents special challenges due to some phenomena that are difficult to control, such as solvent loss,[30] changes in microstructure caused by manipulation,[31] and even wall slip effects.[30,32] In order to avoid a wrong estimation of the rheological properties of our hydrogels due to the effect of these undesired phenomena, we used a double cone-plate geometry (60 mm in diameter and angle of 2º; sensor DC60/2º Ti L, Thermo Fisher Scientific, Waltham, MA, USA) for the characterization of the rheological properties, and we generated each of the hydrogels directly inside this geometry prior to measurement. For this aim, we prepared the hydrogel-precursor mixture and immediately afterwards we poured it in the cup of the measuring geometry, lowered down the double cone and covered with the upper plate. To avoid water evaporation, we created a supersaturated water atmosphere around the measuring geometry. Then, the mixture was left to gelation for 24 hours at 25 ºC. For the application of a magnetic field during the initial steps of gelation, we used a coil placed coaxially with the axis of the double cone. After the 24 h period, we carried out the rheological characterization at 25 ºC, without any prior preshear or manipulation, thus ensuring unspoiled microstructure of the hydrogel. For each formulation we measured at least 3 different samples to ensure statistical significance of our results. We provide in this work mean values and standard deviations of each magnitude. For a complete rheological characterization, we carried out different rheological tests, described in the following paragraphs.

Gelation kinetics. During the 24 hours gelation process, we monitored the evolution of the viscoelastic moduli (storage modulus, G', and loss modulus, G'') as a function of time, resulting from an oscillatory shear strain of amplitude 0.001 and frequency 1 Hz. Note that application of a low amplitude oscillatory shear is common practice to analyze sol-gel transitions –see for example the work by Winter.[33] The amplitude used in our work is up to one order of magnitude smaller than amplitudes used in previous works for a similar purpose,[34] and should be low enough to ensure that the building of the gel microstructure was unperturbed. In fact, we verified that the rheological parameters of hydrogels not subjected to this oscillatory shear during gelation were not statistically different from those obtained for hydrogels subjected to it.

Rheological behavior under steady shear stress. After the 24 h gelation period was completed, we subjected the samples to ramps of step-wise increasing shear stress and the corresponding values of the shear strain were obtained. We maintained each value of the shear stress for 10 s. The initial slope of the shear stress vs. shear strain is the rigidity modulus of the hydrogels.

Rheological behavior under oscillatory shear strain. After the 24 h gelation period was completed, we subjected the samples to oscillatory shear strain in order to characterize their viscoelastic response. First, we carried out ramps of oscillatory strains of fixed frequency (1 Hz) and increasing amplitude. Such kind of measurements allows the identification of the linear viscoelastic region (LVR) as the low range of values of the strain amplitude for which the viscoelastic moduli (both G' and G'') are approximately independent of the magnitude of the strain amplitude. Above the LVR, G' decreases abruptly

with the strain amplitude, whereas G'' usually increases first and then decreases. These changes in the values of G' and G'' mark the onset of the nonlinear viscoelastic region.[35] Once we delimited the LVR, we subjected the samples to ramps of constant shear strain amplitude (we chose the value 0.002, well within the LVR) and increasing frequency in the range 0-10 Hz. From these measurements, we obtained the trends of G' and G'' as a function of frequency, in the LVR.

Analysis of the mechanical anisotropy of the magnetic hydrogels. In order to analyze if the magnetic hydrogels gelled under a magnetic field presented anisotropic mechanical properties, we carried out additional rheological measurements using parallel plate geometry. We used parallel plate geometry (instead of double cone-plate geometry) for these measurements since it was not possible to apply a magnetic field perpendicular to the axis of the rheometer due to set-up limitations. We proceeded as it follows. We prepared the hydrogels (without FeNPs and containing 0.3 vol.% of FeNPs) on disposable bottom plates (made of aluminum) of the rheometer, on which we previously carved a cylindrical hole of 2 mm of depth and 35 mm of diameter to avoid spreading of the content. The hydrogels were gelled for 24 hours under water saturated atmosphere following the same protocol described above. In the case of magnetic hydrogels we applied a magnetic field of 15 kA·m^{-1} of strength (with the help of a solenoid), either perpendicular (vertical) or parallel (horizontal) to the plane of the plate, during the first hour of gelation. After 24 hours we placed the plate containing the hydrogel in the rheometer and descended the upper plate (35 mm in diameter; serrated surface to avoid wall slip) until perfect contact with the hydrogel was reached, without appreciable compression. Afterwards we carried out measurements under steady shear stress and under oscillatory shear strain, following the same protocols described above.

Results and discussion

Characterization of the magnetic particles

TEM micrographs revealed that FeNP powders were composed of spherical particles with a broad distribution in size (see Figure S2 of the ESI). Indeed, particle size distribution of MNP fitted well to a Gaussian distribution (Figure S3 of the ESI), typical of particles resulting from growth starting from nuclei with negligible agglomeration.[36] The best fit to a Gaussian distribution function provided a mean diameter ± standard deviation of 73 ± 20 nm. TEM pictures also demonstrate the successful coating of the MNP@PEG by a thin layer of PEG (Figure S2 of the ESI). Furthermore, the existence of a PEG layer around the particles was corroborated by measurements of the electrophoretic mobility of the nanoparticles (Figure 2). As observed, the electrophoretic mobility significantly decreased for MNP@PEG with respect to PMNP for the whole range of pH values under study (from pH 4 to pH 11). Furthermore, the isoelectric point (zero mobility) for PMNP is closed to the characteristic value of hematite (pH 7),[37] which is the iron oxide expected at the surface of iron. On the other hand, the isoelectric point of MNP@PEG is close to pH 4, considerably lower than this of PMNP. This is coherent with a PEG coating, since in this case the surface of the nanoparticles is functionalized by hydroxyl groups and, thus, a trend to negative mobility is expected, as observed. Consequently, we can conclude that the particles were successfully coated by a PEG layer after treatment. In addition, the mobility was decreased even further after treatment with Fmoc-FF, which corroborates the adsorption of these molecules on the MNP@PEG, also inferred from spectrophotometric measurements as mentioned above. Note that for MNP@PEG@Fmoc-FF measurements at pH 9 or smaller were impossible due to the formation of a gel. The treatment of MNP@PEG with Fmoc-FF peptide was carried out to improve the dispersion of the particles in the solution to originate homogeneous gels. In fact, when MNP@PEG particles were not pre-treated with Fmoc-FF an inhomogeneous gel was obtained (data not shown). In this sense, all the experiments conducted in the hydrogels and discussed in the following subsections have been performed with these MNP@PEG@Fmoc-FF particles, for simplicity, sometimes mentioned as FeNPs.

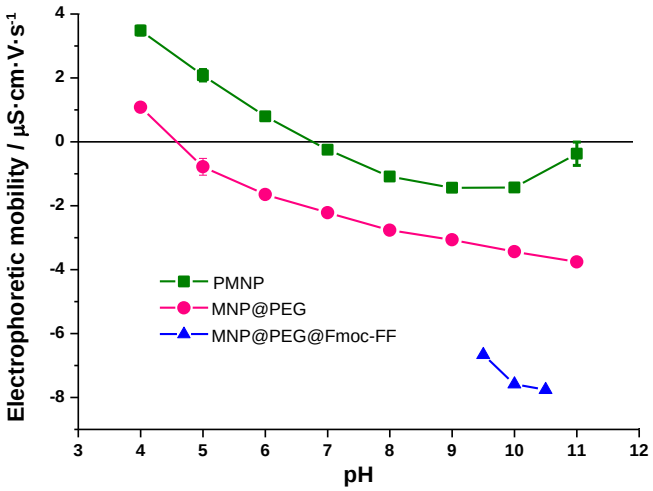

Figure 2. Electrophoretic mobility of the nanoparticles.

Magnetization studies

The magnetization curve of the iron powders demonstrated a typical ferromagnetic behavior for both PMNP and MNP@PEG (Figure S4 of the ESI). From these curves we obtained the values of the saturation magnetization (1521 ± 15 kA·m^{-1} for PMNP and 1530 ± 12 kA·m^{-1} for MNP@PEG) and the values of the remnant magnetization (62.3 ± 2.4 kA·m^{-1} for PMNP and 75 ± 3 kA·m^{-1} for MNP@PEG). From these data, as well as for the general shape of the magnetization curves (Figure S4 of the ESI), we may conclude that the coating by PEG has an almost negligible effect on the magnetic properties of the iron powder. Furthermore, in both cases a rather soft ferromagnetic behavior is evidenced. The slightly higher values of saturation magnetization and remnant magnetization in the case of MNP@PEG with respect to PMNP can be attributed to protection against oxidation due to the coating with PEG –in

the case of PMNP a thicker layer of nonmagnetic oxide is expected at the surface.

Magnetization curves of magnetic hydrogels presented a similar shape to these of MNP@PEG, although with a much smaller saturation magnetization (Figure 3). From these curves we obtained the volume concentration of magnetic particles (ϕ) within the hydrogels using the mixing law of magnetism:[38] $M_{sh}=\phi \cdot M_s$, with M_{sh} and M_s being the saturation magnetizations of the hydrogels and the MNP@PEG, respectively.

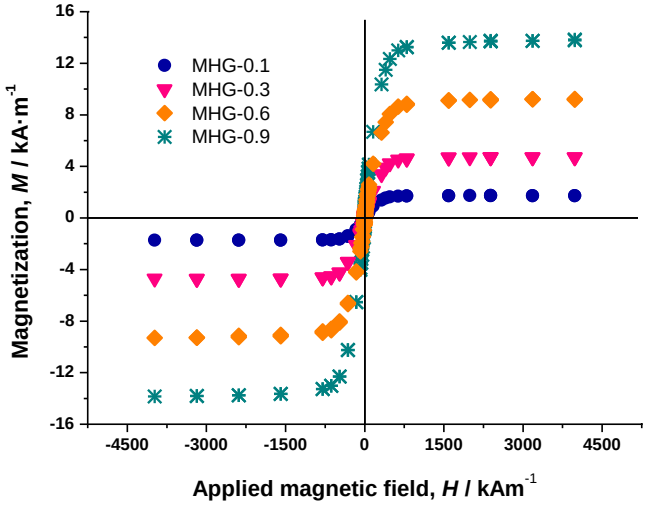

Figure 3. Magnetization curves of magnetic hydrogels.

As observed, there is a good correspondence between concentrations according to preparation protocol and those obtained from magnetization measurements (Table S1 of the ESI).

Morphology characterization

Optical microscopy studies. It is well known that the application of a magnetic field to a liquid-based suspension of magnetic particles induces the reversible formation of particle chain-like structures parallel to the direction of the applied field.[39] Brownian motion destroys such structures after field removal. Then, since we applied a magnetic field of 15 kA·m^{-1} for 1 hour from the very beginning of the start of gelation, we expected that some FeNPs chains were built. Interestingly, as evidenced from optical microscopy (Figure 4), some percolating column-like particle aggregates were observed homogeneously distributed throughout the final MHGs. At this point, question raises on the mechanism because of which the particle structures were maintained even after field removal. The low remnant magnetization of the particles does not justify this observation and, consequently, the reason should be on the interaction with the peptides, as we discuss in the next subsection.

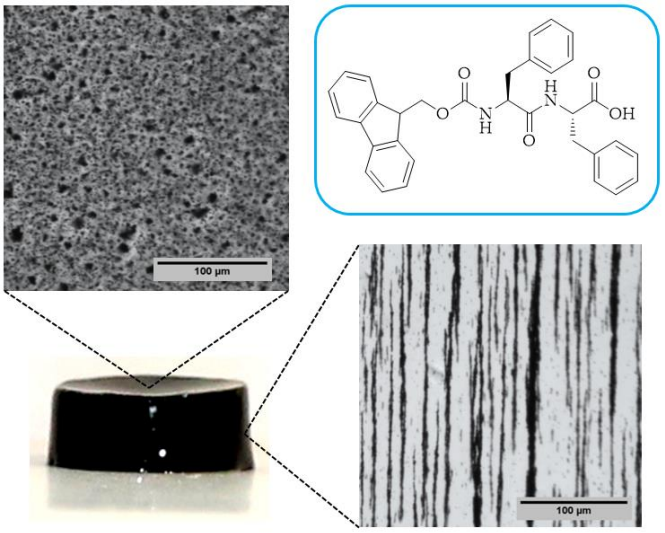

Figure 4. Macroscopic picture of the hydrogel and optical images from the top and side views.

Electron microscopy studies. Fmoc-FF peptide hydrogels have been studied before by electron microscopies.[40] It has been demonstrated that the gel-triggered conditions (solvent or pH switch) have a great impact in the final hydrogel microstructure. Additionally, the non-covalent nature of these aggregates made them very sensitive to external changes. For this reason, simple air-drying or more drastic procedures to obtain the xerogel can have an influence in the final morphology of the fibrils. Although TEM and SEM images of xerogels have been successfully reported showing long nanofibers of 10 nm to 150 nm in diameter,[13] we decided to study the supramolecular arrangements of this peptide and peptide–FeNPs composites directly in the hydrogel medium. To accomplish this objective we used an ESEM coupled with a Peltier to analyze the hydrogels under an optimized temperature (-5 ºC) and humidity (80 %) conditions. As we can see in Figure 5A NMHG shows a dense network of branched ribbons and sheets, which differs significantly from the previously published reports based on xerogels. The tridimensional structure consists of a highly dense porous web with pores of different sizes.

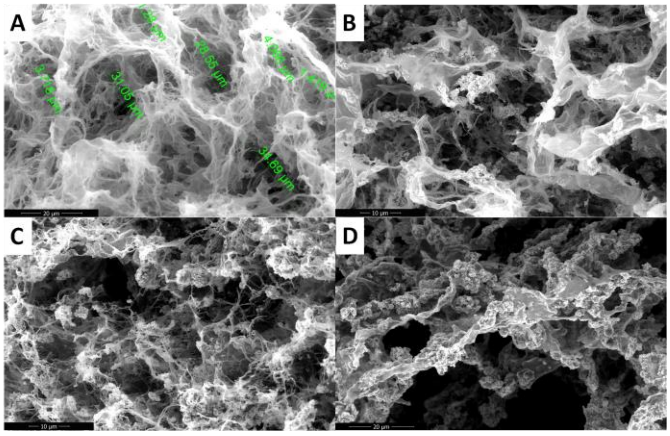

Figure 5. ESEM of NMHG (A) and MHG-0.1 (B), MHG-0.3 (C) and MHG-0.6 (D).

In the case of MHGs we were interested to see whether the Fmoc-dipeptide would be able to maintain the same microstructural order or would be significantly challenged by the presence of the FeNPs considering that the gel is formed in the presence of them. Furthermore, we looked for some clue for the reason of the maintenance of the particle column-like structures (aggregates) after the field removal. As we can see in Figures 5B-D the supramolecular structure of the peptide is maintained in all samples to originate a macroporous web now decorated all over with FeNPs. A possible explanation can be that the FeNPs aggregates are included in the structure simultaneously during fibers and sheets formation. Quite interestingly, the peptide supramolecular arrangement is able to withstand up to 0.6 vol.% FeNPs loading without altering significantly its structure, which is quite impressive considering the small amount of the peptide involved in this process. At the same time, the different particles that constitute each of the column-like aggregates observed by optical microscopy seem to be fixed together by the peptide structure, which would justify the maintenance of the percolating particle aggregates after the magnetic field is switched off. Interestingly, this particular distribution of FeNPs column-like structures within the peptide network drastically reinforces the gel matrix without practically altering the pore size, whilst, at the same time, improves the diffusion of a solute through it, will be seen below.

Secondary structure

Circular dichroism (CD) and Fourier transform infrared spectra (FTIR) were used to analyse and compare the secondary structure of NMHG and MHGs to address the degree of degradability of the supramolecular arrangement of Fmoc-FF dipeptide. For this purpose we carried out both studies in the gel phase. Although CD analysis of these hydrogels could be prone to artifacts and is very sensitive to gel concentration,[40a] we were mainly interested in the comparison between gels. It is also known that the spectra of the hydrogel is also very sensitive to experimental conditions used to prepare it.[41] In this sense, in our experimental conditions (pH switch using GdL) the CD spectrum of NMHG showed a maximum at 221 nm results from n-π transitions and at 279 nm that corresponds to π-π transitions in the fluorenyl groups (Figure 6).

Ulijn and coworkers have suggested that Fmoc-FF may be assembled in a β-sheet structure in the hydrogel prepared by pH switch using HCl.[40a] In our case the n-π transition is slightly shifted to lower wavelength (from 218 nm to 222 nm). This can be due to the different concentration used for both experiments (Ulijn *et al.*: 1.07 wt %) and (this work: 0.3 wt %). This phenomenon has already been described and can only mean that higher peptide concentration indicates the presence of more β-sheet conformation.[42] Quite interestingly, the CD spectra of MHG-0.05 and MHG-0.1 showed a similar shape with the same two peaks at equal wavelengths (Figure 6). These results indicate that the secondary structure derived from the self-assembly of the peptide practically remains unaltered in the presence of the FeNPs at these concentrations. Unfortunately the CD spectra at higher FeNPs concentrations could not be performed due to the light scattering caused by the sample.

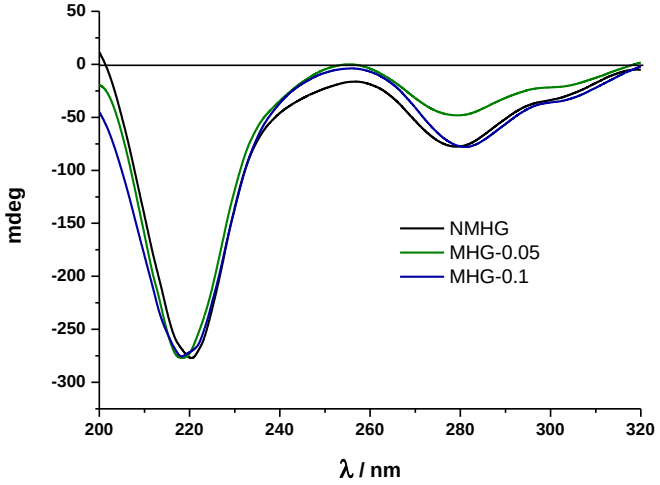

Figure 6. CD spectra of NMHG and MHG-0.05 and MHG-0.1.

To further corroborate these results we performed FTIR of all hydrogels. The FTIR spectrum of NMHG xerogel (Figure 7, dark red line), showed two main peaks at 1651 and 1534 cm^{-1}. These bands can be assigned as the C=O stretching (amide I) and N–H bending (amide II) band respectively.[42] With respect to the corresponding xerogel, the C=O stretching band (amide I) in the hydrogel NMHG (black line) is slightly red shifted (1645 cm^{-1}) and the band of the N–H bending (amide II) is slightly blue shifted (1536 cm^{-1}) indicating the formation of H-bonds.[42,43] Similarly to previous reports,[42,40a] the presence of two amide bands at 1645 and 1536 cm^{-1} indicates a preference for a β-sheet conformation. Additionally, the presence of the band at 1692 cm^{-1} suggests an antiparallel β-sheet arrangement for the self-association of the Fmoc peptide.[42] As we can observe from Figure 7, the FTIR spectra of all MHGs have the same two amide bands at similar wavelengths than the NMHG, which is in agreement with a β-sheet conformation and in line with the results observed in the CD. In this case, the amide I band in all the MHGs is red shifted to 1634 cm^{-1}. This shift can be due to an increase in the H-bond formation between the peptide and the PEG shell of the FeNPs. These results evidence that the dispersion and distribution of FeNPs column-like structures within the gel matrix did not alter significantly the secondary structure of the peptide. This phenomenon can be due to the smaller sizes of the metallic nanoparticles and their columnar aggregates with respect to the higher aspect ratio of the peptide supramolecular network. Also, the rigid FeNPs column-like aggregates located at fixed positions under the influence of an external magnetic field could also minimize the disruption of the peptide self-assembly and secondary structure.

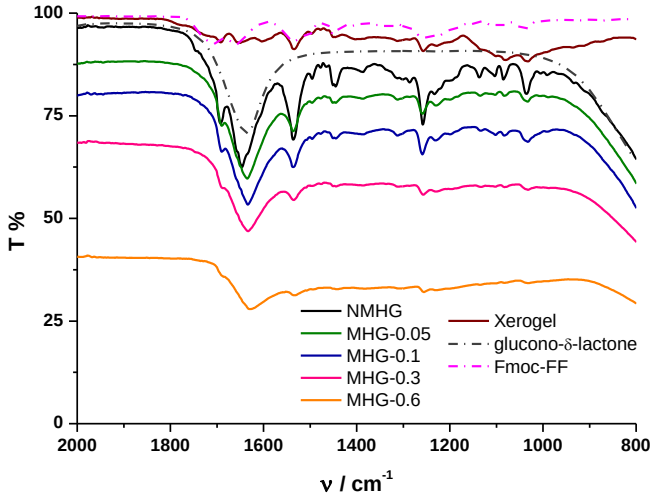

Figure 7. FTIR spectra of Fmoc-FF peptide, GdL, Fmoc-FF xerogel, NMHG and MHGs.

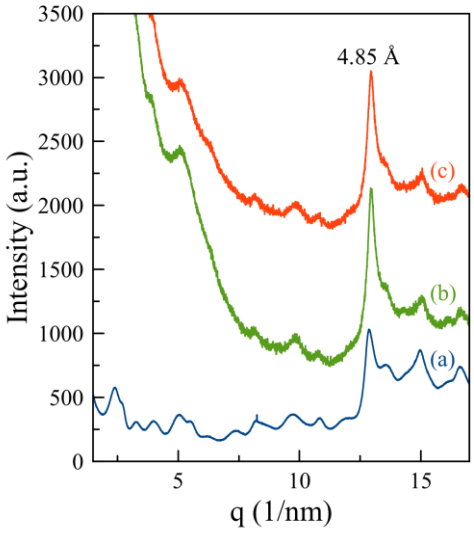

Figure 8. Synchrotron X-Ray Total Scattering patterns of the NMHG (a) and the MHG-0.3 in the absence (b) and presence (c) of magnetic fields.

The XRD pattern of the NMHG (curve a (blue) of Figure S5 of the ESI) is in good agreement with that previously reported for Fmoc-FF gels.[40a,44] It shows a series of diffraction peaks appearing at d-spacing equal to d/n (where 2 < n < 6). These periodic reflections are consistent with the presence of flat ribbons formed by the parallel stacking along their long axis of single fibrils.[40a] Plotting the n-order against the peak position (as scattering vector, q = (2π/λ)sinθ), one can obtain the width of the single fibrils from the slope (inset in Figure S5 of the ESI). From the best lineal fitting we obtained a width of 26.1 Å single fibril, which is in perfect agreement with the values reported for similar gels.[40a] The spacing between peptides within the β-sheets structure, which typically ranges between 4 and 5 Å depending on the peptide sequence,[40a] appears at a d-spacing of 4.8 Å.

Unfortunately, the corresponding signals of the supramolecular structure in the MHG-0.3 (curve b (green line) of Figure S5 of the ESI) are masked by the high scattering signal of the nanoparticles at such small angles (curve b of Figure S5 of the ESI). To solve this problem, we collected the synchrotron X-ray total scattering patterns of the naked and the particle-bearing gels at the X04SA materials science beam-line of the SLS-PSI (Figure 8). The periodic reflections (1 < n < 6) were visible in the pattern of the NMHG (Figure 8 –curve a, blue line), confirming the formation of ribbons of stacked 26 Å-width single fibrils. The spacing between peptides within the β-sheets also appeared at a d-spacing of 4.85 Å. All these features, although poorly defined due to the scattering of the nanoparticles in this angular region, were distinguishable in the patterns of the MHG-0.3 prepared in the absence (Figure 8–curve b, green line) and presence (Figure 8–curve c, orange line) of a magnetic field. Hence, these results indicate that the supramolecular arrangement of the hydrogels is maintained even when they are prepared in the presence of an external magnetic field, in accordance with the CD and FTIR results.

FLCS studies

We were interested in knowing if the pore sizes distribution of the hydrogel network, and hence the diffusion of solutes through them, were significantly modified by the incorporation of the FeNPs. This is a fundamental question since traditional strategies that try to increase the mechanical properties of hydrogels imply a higher cross-linking, with the subsequent reduction in the pore size of the network hampering the diffusion of solutes through it. Alternative strategies, such as those commented in the introduction do not guarantee an increase in the mechanical properties of the hydrogel or a maintenance of the pore size or diffusion unaltered. This can be a serious drawback in certain biotechnological applications such as, *in vivo* drug delivery and in tissue engineering where cells need an adequate diffusion through the gel matrix for the interchange of nutrients and waste substances.

In this sense, the diffusion pattern of a small dye, **4-OMe-PG**, dissolved in the hydrogels was studied using FLCS. We chose this dye because of the low variation of the fluorescence features of fluorinated xanthenes at near-neutral pH.[31,45] The AC and CC correlation curves of the dye in the MHGs showed a diffusional behavior very close to pure diffusion (Figure 9a). Indeed, the α values ranged from 0.8 to 1.2 in the different measurements. Figure 9b shows the α value distributions for the dye in gels carrying different loads of FeNPs. These distributions were fitted to a Gaussian function, in order to obtain the average value and the associated error (as the half-width of the function). The average α values were 1.07 ± 0.13, 1.01 ± 0.09, 1.05 ± 0.10, and 0.93 ± 0.06 for MHG-0.05, MHG-0.1, MHG-0.3 and MHG-0.6, respectively. A statistical comparison with α = 1 showed that the samples with 0.05 vol.%, 0.1 vol.%, and 0.3 vol.% of FeNPs were statistically not different from pure diffusional behavior (*p* value > 0.03). This entails that the **4-OMe-PG** dye diffuses similarly in the hydrogel than in a bulk solvent. Furthermore, the obtained

apparent diffusion coefficients were 380 ± 130, 450 ± 170, and 400 ± 110 μm²/s, for the dye in MHG-0.05, MHG-0.1 and MHG-0.3, respectively. These values are in perfect agreement with the diffusion coefficient obtained for the **4-OMe-PG** dye free in aqueous solution of 410 ± 70 μm²/s, after fitting the FLCS-CC and AC functions to a pure diffusional model (with α = 1). Therefore, these values are in line with the diffusion coefficient of a small dye in aqueous solution, confirming the quasi-aqueous environment of the dye in the hydrogels. However, the population of samples in the MHG-0.6 was statistically different from a pure diffusional behavior with a significance of 99 % (*p* value = 3×10^{-6}). This means that the **4-OMe-PG** dye dissolved in the hydrogel with high loads of FeNPs presents a distinguishable subdiffusion behavior, although not very prominent. The average apparent diffusion coefficient for the dye in this gel was 540 ± 100 μm²/s. The apparent increase in the diffusion coefficient, compared to the other measurements, may be related to the formation of preferential channels for diffusion, restricting the pure 3D random walk of molecules. This effect is similar to the anomalous diffusion found for small dyes in the presence of large concentrations of crowding agents.[46] The excluded volume caused by the external agent makes the diffusion of the dye apparently faster compared to a freely diffusional environment. In any case, the effect is very mild, confirming that the aqueous nature of the hydrogel is mainly maintained, and that the pore size in these gels is larger than the dye's size. As previously reported for agarose gels, when the diffusing dye is much smaller than the gel's pore size, an α value around 0.93 described well the shape of the autocorrelation functions[28] and the dyes diffuse like they were dissolved in homogeneous media. Although the refractive index mismatch between the probe medium and the glass may cause artifacts, such as the detection on an apparent anomalous diffusion behavior,[47] the detected curves are that similar to a pure diffusional model that this effect is likely negligible.

In order to test whether the quasi-aqueous environment for the **4-OMe-PG** dye was promoted by the microscopic structure of the hydrogels being controlled by the long range sorting of the FeNPs column-like aggregates due to the magnetic field, we probed the diffusional behavior of the dye in MHG-0.1 and MHG-0.3 hydrogels, but formed without an external magnetic field, and in the NMHG. Figure 9b shows the α value distributions of the **4-OMe-PG** dye in these cases. Interestingly, the α distributions were very similar in the samples formed with and without the magnetic field. The average α values, obtained from the fits to a Gaussian function, were 0.97 ± 0.11 and 0.99 ± 0.08 for the MHG-0.1 and MHG-0.3 respectively, formed without field. Likewise, the average apparent diffusion coefficient values of the dye in such gels were 440 ± 190 and 410 ± 150 μm²/s, for the MHG-0.1 and MHG-0.3 respectively. The α distributions for these hydrogels were not statistically different from α = 1 (*p* values > 0.4), confirming also the quasi-aqueous environment of the dye in the gels. The most striking result was obtained, however, with the NMHG. The diffusion of the **4-OMe-PG** dye in this gel was clearly anomalous, with an average α = 0.62 ± 0.22 (Figure 9b), suggesting a more intricate micro-environment for the dye.

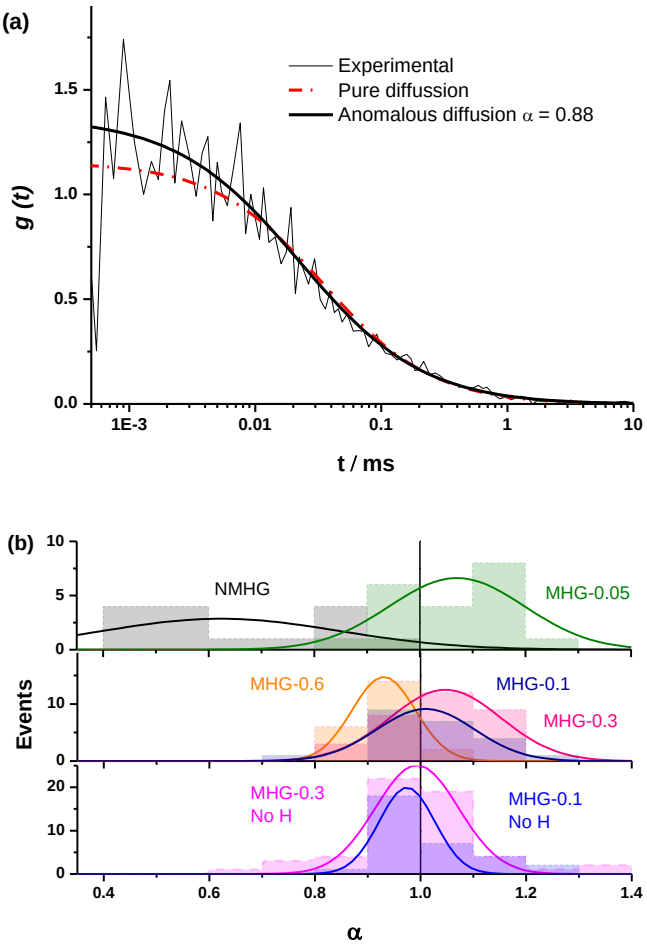

Figure 9. a) Representative FLCS-CC curve of 4-OMe-PG dye in MHG-0.6, fitted to a pure diffusional model and to an anomalous diffusion equation. b) Anomalous diffusion parameter α distributions for the 4-OMe-PG dye in hydrogels without FeNPs (black), with 0.05 vol.% (green), 0.1 vol.% (royal blue), 0.3 vol.% (pink), and 0.6 vol.% (orange) of FeNPs, formed with magnetic field, and in hydrogels with 0.1 vol.% (blue) and 0.3 vol.% (magenta) of FeNPs, formed in the absence of the magnetic field.

In conclusion, a small dye, such as **4-OMe-PG**, finds a quasi-aqueous environment in the gels formed with FeNPs and magnetic field, caused by the formation of preferential channels for diffusion. The formation of hydrogels with FeNPs, but in the absence of magnetic field, leads to a very similar microenvironment. This gel micro-structure largely contrasts with that of the hydrogel without FeNPs, which exhibits a diffusion in agreement with a close and tight network of fibrils. This difference in structures is in agreement with the information obtained in the ESEM images (Figure 5).

Rheological Studies

Gelation kinetics. As described above, we monitored the evolution of G' and G'' as a function of time in order to analyze the kinetics of gelation of our hydrogels. As observed, both G' and G'' increased strongly with time in the initial steps of the

gelation process (up to approx. 200 s) –see results for MHG-0.05 as an example in Figure S6 of the ESI. Afterwards, the increase in moduli continued at lower rate, although there was again a stronger increase around 20000 s. Finally, the values of both G' and G'' leveled off for times larger than approximately 50000 s (approx. 14 hours). Similar trends were obtained for other hydrogels (not shown). Comparison between gelation kinetics for different hydrogels evidenced a faster growth of G' and G'' with time for magnetic hydrogels with respect to nonmagnetic hydrogels, although there was not a clear tendency to a faster gelation kinetics by increasing the content of FeNPs. Furthermore, as observed in Figure S6 of the ESI, from the very beginning of the experiments G' was larger than G'' (characteristic of the presence of a gel-like material), which is an indication of the immediate crosslinking, as soon as the GdL was added. This is not surprising since the addition of the GdL causes the immediate formation of fiber-like structures that interact by overlapping.[24] Nevertheless, completion of the crosslinking process required very long times (more than 12 hours) as evidenced from the fact that the viscoelastic moduli continued to increase very fast during this time.

Rheological behavior under steady shear stress. As observed, within the range of shear strains studied in our work, the shear stress shows an increasing linear trend with the shear strain for both NMHG and MHG (Figure S7 of the ESI). This linear dependence is characteristic of the linear region that viscoelastic materials present at low deformation. The effect of magnetic nanoparticles on the steady state rheological behavior of hydrogels within the linear regime is best described by the slope of shear stress vs. shear strain curves. This slope is the shear (or rigidity) modulus, which is usually used as a measure of the strength of a material. As observed the rigidity modulus of our hydrogels increased strongly with nanoparticle concentration up to 0.1 vol.% (Figure 10). Note that this tiny concentration of nanoparticles provoked a 4-fold increase in the value of the shear modulus with respect to the hydrogel without nanoparticles. Above this concentration and up to 0.6 vol.% the shear modulus still increased, although at a lower rate. However, a further increase in nanoparticle concentration did not provoke any additional enhancement of the shear modulus, but rather a tendency to decrease. Note that associated to the saturation of the mechanical enhancement at high nanoparticle content (0.9 vol.%), there was a lack of homogeneity and preparation became more difficult. Note also that when a magnetic field was not applied during gelation, we did not obtain any enhancement of the rigidity modulus (or other mechanical parameters) with respect to NMHG. Such a global trend, with an initial enhancement of mechanical strength of gels when nanoparticles are added at a low concentration, followed by a leveling off (or even decrease) of the mechanical strength at larger concentrations, has been previously reported in the case of polymeric gels.[48,49] Bonhome-Espinosa et al. found that the enhancement of the mechanical strength observed when nanoparticles were added was due to their role as knots for the crosslinking of the polymer fibers.[49] At larger concentrations of nanoparticles, the polymer network was so much disturbed by the presence of nanoparticles that the formation of a 3-D network of polymer chains started to fail, and thus their mechanical strength diminished.

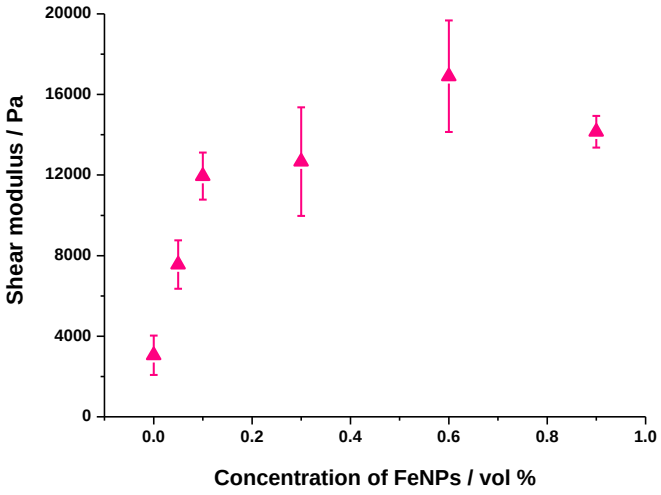

Figure 10. Variation of shear modulus with nanoparticle concentration.

In the case of the present work a different hypothesis should be given since the secondary structure of the peptide hydrogel was practically unperturbed by the introduction of the particles. As discussed before, some column-like particle aggregates were induced by the magnetic field at the start of gelation. Then, during the peptide gel formation, the FeNPs were assimilated within the peptide structure, which was able to withstand the column-like aggregates, as evidenced by optical microscopy (Figure 4). Our hypothesis is that these column-like particle aggregates served as some microscopic scaffold on which the secondary structure of the peptide gel was supported, giving a superior mechanical strength to the resulting hydrogels. From the optical microscopy, it is evident that the resulting particle structures are percolating. Furthermore, from the theoretical point of view, the following analysis can be made. In a first approximation, the particle structures induced by the field can be considered as long cylinders aligned in the direction of the applied field (unit vector $\boldsymbol{e}_1$), whereas the applied shear stress is τ_{12}. Then, according to the most common model for the mechanical properties of composite materials with cylinder inclusions, introduced by Hashin and Rosen,[50] we have the following expression for the shear modulus of the composite in the cylinder direction, G_{12}:

$$G_{12} = G_m \frac{G_c(1+\Phi)+G_m(1-\Phi)}{G_c(1-\Phi)+G_m(1+\Phi)} \qquad (2)$$

Where G_m and G_c are respectively the shear modulus of the continuous matrix and the cylinders (nonmagnetic peptide hydrogel and elongated particle aggregates in the present work), and Φ is the volume fraction of the cylinders (that should be of the same order of magnitude than the volume fraction of the magnetic nanoparticles). However, from this expression it is evident that even for completely rigid cylinders ($G_c \to \infty$), the enhancement in the G_{12} with respect to G_m is

almost negligible for Φ of the order of 0.01, as in the present work. However, if we have percolating structures, we may approximate the shear modulus of the composite in the cylinder direction by this of a mixture, which is given by:[18]

$$G_{12} = \Phi G_c + (1-\Phi) G_m \quad (3)$$

This trend predicted by formula (3) fits perfectly the experimental data for the shear modulus corresponding to volume fractions up to 0.001 (Adj. R-Square equal to 0.99991), with G_c=92100 ± 600 Pa and G_m=3060 ± 40 Pa. These data indicate that the shear modulus of the particle structures should be about 30 times stronger than the shear modulus of the peptide hydrogel, which seems reasonable taking into account that magnetic nanoparticles made of iron are interpenetrated and interwoven by the self-assembled peptide. This composite material originates a structure similar to reinforced concrete, in which a skeleton of steel wires are filled with cement. Concerning the tendency of the shear modulus to level off at volume fractions higher than 0.001, the likely reason is the progressive difficulty of the peptides to give consistence to the particle structures and to hold them.

Rheological behavior under oscillatory shear strain. The trend of G' and G'' as a function of shear strain amplitude for oscillatory experiments at a fixed frequency of 1 Hz demonstrated a typical behavior of cross-linked systems –see as an example trend for MHG-0.05 in Figure S8 of the ESI; similar trends were obtained for other hydrogels. As observed, at low enough shear strain amplitude, both G' and G'' present an almost constant value. This region is identified with the linear viscoelastic regime (LVR). Within the LVR, G' is much larger (almost two orders of magnitude) than G''. In other words, the elastic response of the hydrogel (storage of energy) dominates over its viscous response (loss of energy), as expected for cross-linked systems. At larger values of the strain amplitude, G'' exhibits a rather noticeable enhancement, followed by a maximum for an approximate strain amplitude of 0.03. This maximum in G'' (maximum in loss of energy) corresponds to the yielding (irreversible destruction) of the hydrogel.[35] For even larger values of the strain amplitude both G' and G'' decrease strongly and eventually they cross at large enough strain amplitude. Additionally, we performed oscillatory measurements of the hydrogels after extrusion through a syringe and confirmed that the hydrogels (both magnetic and nonmagnetic) retained their gel-like nature, characterized by G' values higher than G'' within the LVR (Figure S9 of the ESI).

As mentioned above, all hydrogels (magnetic and nonmagnetic) of the present work presented a similar trend of G' and G'' as a function of strain amplitude. The main difference was the relative values of these magnitudes that increased strongly with FeNPs concentration up to 0.1 vol.%, and then at a smaller rate with a tendency to level off at concentrations above 0.6 vol.% –see a plot with the values corresponding to the LVR in Figure 11. Note that an increase of G' of approx. 7 times is obtained for the highest concentration of FeNPs (0.9 vol.%) with respect to the NMHG. This trend is similar to the one discussed above for the shear modulus.

Other parameters that depend on FeNPs concentration are the amplitudes of the shear strain and the shear stress corresponding to the yield point (peak value of G'' in curves like this of Figure S8 of the ESI). In the case of these hydrogels, the shear strain at the yield point showed a tendency to decrease as the content of FeNPs increased, whereas the shear stress at the yield point increased with FeNPs content (Figure S10 of the ESI). We obtained similar trends (not shown here) for the critical shear strain and critical shear stress that marked the onset of the nonlinear viscoelastic region. In overall terms, we can conclude that as FeNPs are included at a larger proportion in the composition of these supramolecular hydrogels (prepared under an applied magnetic field), the resulting magnetic hydrogels become tougher and, accordingly, their strain at fracture diminishes.

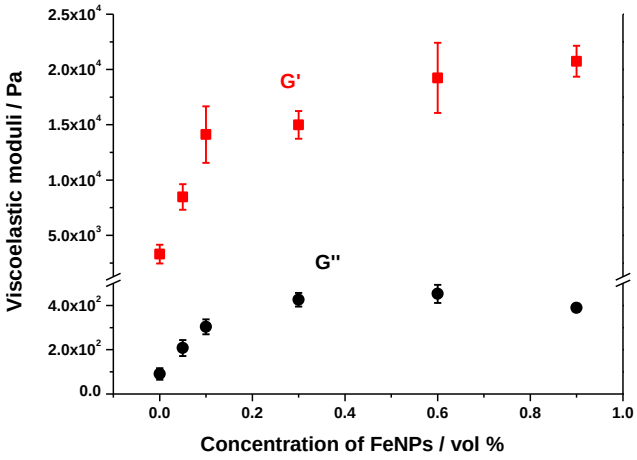

Figure 11. Representation of viscoelastic moduli against concentration of FeNPs.

Finally, we also obtained the oscillograms (curves of G' and G'' as a function of frequency of oscillatory shear strain) corresponding to the LVR (Figure 12). As observed, trends are similar for NMHG and MHGs, independently of the concentration of magnetic nanoparticles, being the values of G' and G'' the only distinctive difference between curves corresponding to different hydrogels. In all cases, G' showed a constant value within the whole range of frequencies under study. As for G'', first it increased smoothly with frequency, then it reached a maximum around a frequency of 4 Hz, afterwards it decreased sharply, and finally showed a tendency to level off at the highest frequencies. The independence of G' on the frequency of the oscillatory shear, as well as the smooth increase of G'' with frequency, are typical of strongly cross-linked systems, like rubber.[51] Concerning the decrease of G'' observed around 4 Hz, it has been previously observed for polymer hydrogels.[49]

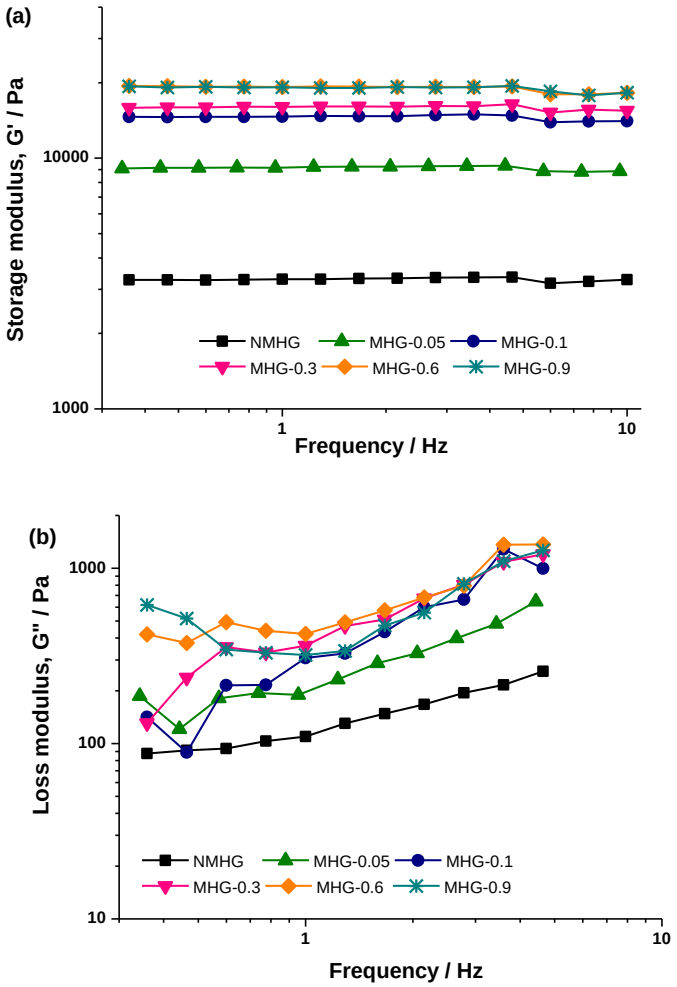

Figure 12. Oscillograms corresponding to the LVR of NMHG and MHGs: (a) storage modulus *vs* frequency and (b) loss modulus *vs* frequency.

Analysis of the mechanical anisotropy of the magnetic hydrogels. These magnetic hydrogels present a clear anisotropic behavior, evidenced by smaller rheological moduli that the NMHG when the shear was applied in the same plane as the magnetic field, and higher rheological moduli when the shear was applied perpendicular to the direction of the magnetic field (Table 1). This anisotropy highlights the strong influence that the FeNPs column–like aggregates have in the final macroscopic mechanical properties of the hydrogels.

Table 1. Data of storage and loss moduli for MHG-0.3 prepared under horizontal (MHG-0.3H) or vertical (MHG-0.3V) magnetic field, with respect to the plane of the disk-like hydrogel and the plane of shear. For comparison data for NMHG are also included. Similar trends were obtained for the shear modulus, not shown here for brevity.

Hydrogel	Storage modulus (Pa)	Loss modulus (Pa)
NMHG	2960 ± 160	209 ± 8
MHG-0.3H	1120 ± 120	124 ± 13
MHG-0.3V	5900 ± 300	352 ± 23

Conclusions

Novel short-peptide supramolecular magnetic hydrogels have been prepared by the self–assembly of Fmoc-FF in a suspension containing iron nanoparticles (FeNPs) in the presence or absence of an external magnetic field. The influence of the magnetic field modifies the structural characteristics of the hydrogels inducing the formation of FeNPs column-like aggregates. The resulting anisotropic structure composed of vertically aligned FeNPs columns-like aggregates engulfed by the peptide fibers is the responsible of the enhancement in the mechanical properties of these hydrogels. As far as we know, this is the first time that such enhancement in the mechanical properties of a supramolecular hydrogel is mediated by the presence of FeNPs, and can only be explained due to the particular characteristics of this material, in which, the non-covalent nature of the peptide self-assembly is essential. Quite interestingly, the peptide β-sheet secondary structure is conserved as well as the pore size, being this one of the few examples in which the mechanical strength of the gel is enhanced without altering significantly the microstructure of the gel network and improving the diffusion of a solute through it.

Conflicts of interest

There are no conflicts of interest to declare.

Acknowledgements

This study was supported by projects CTQ-2014-53598-R and FIS2013-41821-R (Plan Nacional de Investigación Científica, Desarrollo e Innovación Tecnológica, MINECO (Spain), co-funded by ERDF, European Union), FIS2017-85954-R (Agencia Estatal de Investigación, AEI, Spain, co-funded by Fondo Europeo de Desarrollo Regional, ERDF, European Union) and by Junta de Andalucía (Spain) project P12-FQM-2721.

References

1 (a) M. Ebara et al., Smart Biomaterials, NIMS Monographs, DOI: 10.1007/978-4-431-54400-5, National Institute for Materials Science, Japan. Published by Springer Japan 2014; (b) A. Döring, W. Birnbaum and D.Kuckling, *Chem. Soc. Rev.,* 2013, **42**, 7391.

2 (a) E. I. Anastasova, V. Ivanovski, A. F. Fakhardo, A. I. Lepeshkin, S. Omar, A. S. Drozdov and V. V. Vinogradov, *Soft Matter*, 2017, **13**, 8651; (b) A. Campanella, O. Holderer, K. Raftopoulos, C. Papadakis, M. Staropoli, M. Appavou, P. Müller-Buschbaum and H. Frielinghaus, Nanotechnology (IEEE-NANO), 2016 IEEE 16th International Conference on, 2016, 446; (c) J. Thévenot, H. Oliveira, O. Sandre and S. Lecommandoux, *Chem. Soc. Rev.,* 2013, **42**, 7099.

3 (a) Y. Li, G. Huang, X. Zhang, B. Li, Y. Chen, T. Lu, T. J. Lu and F. Xu, *Adv. Funct. Mater.* 2013, **23**, 660; (b) J. Zhang, S. Xu and E. Kumacheva, *J. Am. Chem. Soc.*, 2004, **126**, 7908.

4 (a) C. D. Jones and J. W. Steed, *Chem. Soc. Rev.,* 2016, **45**, 6546; (b) X. Du, J. Zhou, J. Shi, and B. Xu, *Chem. Rev*. 2015, **115**, 13165−13307.
5 A. Wang, W. Shi, J. Huang and Y. Yan, *Soft Matter,* 2016, **12**, 337.
6 (a) K. Tao, A, Levin, L. Adler-Abramovich and E. Gazit, *Chem. Soc. Rev.,* 2016, **45**, 3935; (b) S. Fleming, R. V. Ulijn, *Chem. Soc. Rev.,* 2014, **43**, 8150; (c) A. Dasgupta, J. H. Mondal and D. Das, *RSC Advances*, 2013, **3**, 9117.
7 E. R. Draper and D. J. Adams, *Chem* 2017, **3**, 390.
8 (a) D. J. Cornwell and D. K. Smith, *Mater. Horiz*., 2015, **2**, 279; (b) M. Conejero-Muriel, R. Contreras-Montoya, J. J. Díaz-Mochón, L. Álvarez de Cienfuegos, J. A. Gavira. *CrystEngComm,* 2015, **17**, 8072; (c) M. Conejero-Muriel, J. A. Gavira, E. Pineda-Molina, A. Belsom, M. Bradley, M. Moral, J.-D. García-López Durán, A. Luque González, J. J. Díaz-Mochón, R. Contreras-Montoya, Á. Martínez-Peragón, J. M. Cuerva, and L. Álvarez de Cienfuegos. *Chem. Commun.,* 2015, **51**, 3862.
9 (a) J. Raeburn, C. Mendoza-Cuenca, B. N. Cattoz, M. A. Little, A. E. Terry, A. Z. Cardoso, P. C. Griffiths and D. J. Adams, *Soft Matter*, 2015, **11**, 927; (b) J. Raeburn, G. Pont, L. Chen, Y. Cesbron, R. Levy and D. J. Adams, *Soft Matter*, 2012, **8**, 1168; (c) L. Chen, J. Raeburn, S. Sutton, D. G. Spiller, J. Williams, J. S. Sharp, P. C. Griffiths, R. K. Heenan, S. M. King, A. Paul, S. Furzeland, D. Atkins and D. J. Adams, Soft Matter, 2011, **7**, 9721; (d) W. Helen, P. D. Leonardis, R. V. Ulijn, J. Gough and N. Tirelli, *Soft Matter*, 2011, **7**, 1732.
10 (a) V. Jayawarna, S. M. Richardson, A. R. Hirst, N. W. Hodson, A. Saiani, J. E. Gough and R. V. Ulijn, *Acta Biomater*., 2009, **5**, 934; (b) M. Zhou, A. M. Smith, A. K. Das, N. W. Hodson, R. F. Collins, R. V. Ulijn and J. E. Gough, *Biomaterials*, 2009, **30**, 2523.
11 (a) G. Pont, L. Chen, D. G. Spiller and D. J. Adams, *Soft Matter*, 2012, **8**, 7797; (b) L. Chen, S. Revel, K. Morris, D.G. Spiller, L. C. Serpell and D. J. Adams, *Chem. Commun.,* 2010, **46**, 6738.
12 J. Wang, Z. Wang, J. Gao, L. Wang, Z. Yang, D. Kong and Z. Yang, *J. Mater. Chem*., 2009, **19**, 7892.
13 R. Huang, W. Qi, L. Feng, R. Su and Z. He, *Soft Matter*, 2011, **7**, 6222.
14 J. Nanda, B. Adhikari, S. Basak, and A. Banerjee, *J. Phys. Chem. B* 2012, **116**, 12235.
15 S. Roy and A. Banerjee, *RSC Advances*, 2012, **2**, 2105.
16 B. Adhikari and A. Banerjee, *Soft Matter*, 2011, **7**, 9259.
17 M. Ikeda, S. Ueno, S. Matsumoto, Y. Shimizu, H. Komatsu, K.-i. Kusumoto, and I. Hamachi, *Chem. Eur. J.,* 2008, **14**, 10808.
18 R.M. Christensen. *Mechanics of Composite Materials*. Krieger Publishing Company, Malabar, 1991.
19 M. C. Nolan, A. M. Fuentes Caparrós, B. Dietrich, M. Barrow, E. R. Cross, M. Bleuel, S. M. King and D. J. Adams, *Soft Matter*, 2017, **13**, 8426.
20 Z. Yang, H. Gu, J. Du, J. Gao, B. Zhang, X. Zhang and B. Xu, *Tetrahedron,* 2007, **63**, 7349.
21 L. Rodriguez-Arco, I. A. Rodriguez, V. Carriel, A. B. Bonhome-Espinosa, F. Campos, P. Kuzhir, J. D. G. Duran and M. T. Lopez-Lopez, *Nanoscale*, 2016, **8**, 8138.
22 (a) R. Petros and J. M. De Simone, *Nat. Rev. Drug Discovery*, 2010, **9**, 615; (b) M. Arruebo, M. Galan, N. Navascues, C. Tellez, C. Marquina, M. R. Ibarra and J. Santamaria, *Chem. Mater.*, 2006, **18**, 1911; (c) H. Otsuka, Y. Nagasaki and K. Kataoka, *Adv. Drug Delivery Rev.*, 2012, **64**, 246.
23 J. Chatterjee, M. Bettge, Y. Haik and C. J. Chen, *J. Magn. Magn. Mater.*, 2005, **293**, 303.
24 D. J. Adams, L. M. Mullen, M. Berta, L. Chena and W. J. Frith, *Soft Matter*, 2010, **6**, 1971.
25 V. Puente-Muñoz, J. M. Paredes, S. Resa, A. M. Ortuño, E. M. Talavera, D. Miguel, J. M. Cuerva, L. Crovetto, *Sensor Actuat. B-Chem*., 2017, **250**, 623.
26 M. Wahl, R. Erdmann, K. Lauritsen, H. J. Rahn, *Proc. SPIE* 1998, **173**, 3259.
27 (a) S. Rüttinger, P. Kapusta, M. Patting, M. Wahl, R. Macdonald, *J. Fluoresc.,* 2010, **20**, 105; (b) P. Kapusta, M. Wahl, A. Benda, M. Hof, J. Enderlein, *J. Fluoresc.,* 2007, **17**, 43.
28 N. Fatin-Rouge, K. Starchev, and J. Buffle, *Biophysical Journal* 2004, **86**, 2710.
29 J. M. Paredes, S. Casares, M. J. Ruedas-Rama, E. Fernández, F. Castello, L. Varela-Álvarez, A. Orte, *Int. J. Mol. Sci.* 2012, **13**, 9400.
30 J. M. Piau, *J. Non-Newtonian Fluid Mech.*, 2007, **144**, 1.
31 D. Bonn and M. M. Denn, *Science*, 2009, **324**, 1401.
32 S. Aktas, D. M. Kalyon, B. M. Marin-Santibanez and J. Perez-Gonzalez, *J. Rheol.*, 2014, **58**, 513.
33 H. H. Winter*, Polym. Eng. Sci*., 1987, **27**, 1698.
34 J. Cho, M. C. Heuzey and M. L. Hamdine, *Macromol. Mater. Eng.*, 2007, **292**, 571.
35 E. Moghimi, A. R. Jacob, N. Koumakis and G. Petekidis, *Soft Matter*, 2017, **13**, 2371.
36 K. Kimura, *In Fine particles*. Marcel Dekker, Inc. 513-551, 2000.
37 K. Quast*, International Journal of Mining Engineering and Mineral Processing*, 2012, **1**, 73-83.
38 R. E. Rosensweig, *Ferrohydrodynamics*. Cambridge University Press, Cambridge, 1985.
39 G. Bossis, O. Volkova, S. Lacis and A. Meunier, *Lect. Notes Phys.*, 2002, **594**, 201.
40 (a) A. M. Smith, R. J. Williams, C. Tang, P. Coppo, R. F. Collins, M. L. Turner, A. Saiani and R. V. Ulijn, *Adv. Mater.*, 2008, **20**, 37; (b) A. Mahler, M. Reches, M. Rechter, S. Cohen and E. Gazit, *Adv. Mater*., 2006, **18**, 1365.
41 B. Ding, Y. Li, M. Qin, Y. Ding, Y. Cao and W. Wang, *Soft Matter*, 2013, **9**, 4672.
42 B. Adhikari, G. Palui and A. Banerjee, *Soft Matter*, 2009, **5**, 3452.
43 A. Banerjee, G. Palui and A. Banerjee, *Soft Matter*, 2008, **4**, 1430.
44 X. Mu, K. M. Eckes, M. M. Nguyen, L. J. Suggs, and P. Ren, *Biomacromolecules*, 2012, **13**, 3562.
45 (a) L. F. Mottram, S. Boonyarattanakalin, R. E. Kovel, B. R. Peterson, *Org. Lett.* 2006, **8**, 581; (b) A. Orte, L. Crovetto, E. M. Talavera, N. Boens, J. M. Alvarez-Pez, *J. Phys. Chem. A* 2005, **109**, 734.
46 (a) S. Smith, C. Cianci and R. Grima, *J. R. Soc. Interface* 2017, 14, 0047; (b) H. Sanabria, Y. Kubota, and M. N. Waxham *Biophysical Journal*, 2007, **92**, 313.
47 S. Lehmann, S. Seiffert, W. Richtering, *Macromol. Chem. Phys.* 2015, **216**, 156.
48 D. Borin, D. Günther, C. Hintze, G. Heinrich, S. Odenbach *Journal of Magnetism and Magnetic Materials*, 2012, **324**, 3452.
49 A. B. Bonhome-Espinosa, F. Campos, I. A. Rodriguez, V. Carriel, J. A. Marins, A. Zubarev, J. D. G. Duran and M. T. Lopez-Lopez, *Soft Matter*, 2017, **13**, 2928.
50 Z. Hashin, B. W. Rosen, *J. Appl. Mech.,* 1964, **31**, 223.
51 C. W. Macosko, *Rheology: principles, measurements and applications*, Wiley-VCH, Weinheim, 1994.

